The FEBS Journal

FEBS PRESS science publishing by scientists

Differential specificity of SARS-CoV-2 main protease variants on peptide versus protein-based substrates

Fernanda R. Rocho[1,2], Scott J. Snipas[1], Anwar Shamim[2], Wioletta Rut[3], Marcin Drag[3], Carlos A. Montanari[2] and Guy S. Salvesen[1]

1 Cell and Molecular Biology of Cancer Program, Sanford Burnham Prebys Medical Discovery Institute, La Jolla, CA, USA
2 Medicinal and Biological Chemistry Group of the Department of Chemistry and Molecular Physics, University of São Paulo, Brazil
3 Department of Chemical Biology and Bioimaging, Wroclaw University of Science and Technology, Poland

Keywords
SARS-CoV-2 M^{pro}; SARS-CoV-2 variants; substrate specificity

Correspondence
F. R. Rocho, Chemistry and Molecular Physics Graduate Program, University of São Paulo, 400 Avenida trabalhador São Carlense, São Carlos, São Paulo, Brazil
Tel: +55 48 998165388
E-mail: fernandareis@usp.br
G. S. Salvesen, Cell and Molecular Biology of Cancer Program, Sanford Burnham Prebys Medical Discovery Institute, 10901 North Torrey Pines Road, C4 92024, La Jolla, CA, USA
Tel: +1 858-646-3200
E-mail: gsalvesen@sbpdiscovery.org

(Received 27 May 2023, revised 17 August 2023, accepted 5 October 2023)

doi:10.1111/febs.16970

The SARS-CoV-2 main protease (M^{pro}) holds significant importance as a biological target in combating coronaviruses due to its importance in virus replication. Considering the emergence of novel SARS-CoV-2 variants and the mutations observed in the M^{pro} sequence, we hypothesized that these mutations may have a potential impact on the protease's specificity. To test this, we expressed M^{pro} corresponding to the original strain and variants Beta1, Beta2, and Omicron and analyzed their activity on protein-based and peptide substrates. Although we observed differential activity on the protein-based substrate, there was very little difference when analyzed on the peptide substrate. We conclude that mutations on the M^{pro} sequence, despite having a minor effect on a peptide substrate cleavage, did not change the catalytic site environment enough to build resistance to inhibition. Therefore, we propose that inhibitors initially designed for the M^{pro} of the original strain will be effective in all the variants. Thus, M^{pro} is likely to continue to be a target of therapeutic interest as mutations in its sequence are rare and, as we show here, have a minor effect on the protease's recognition of peptide-based molecules.

Introduction

In 2019, a new and highly infective coronavirus SARS-CoV-2 emerged, which made the World Health Organization declare a world pandemic on 11 March 2020 [1]. The human coronaviruses (HCoVs) are positive-stranded RNA viruses that are the leading causes of upper respiratory tract illness in humans. The HCoV genome encodes several nonstructural proteins that are synthesized as two large polyproteins pp1a and pp1ab, which are cleaved by the virus proteases named papain-like protease and the main protease (M^{pro}; EC3.4.22.69) [2].

The protease's primary role is to process the polyproteins pp1a and pp1ab, which mediate the functions required for viral replication and transcription [1,3–5], and possibly also cleavage of host proteins [6,7]. The enzyme has a very stringent cleavage specificity, recognizing preferentially the sequence Leu-Gln↓ (Ser, Ala, Gly) [3,8]. Thus, due to its vital role and cleavage specificity, M^{pro} has become a key target for developing antiviral drugs [9,10]. Paxlovid was the first approved drug for the treatment of COVID-19 that targets M^{pro} with high affinity [11]. The drug is composed of the M^{pro}

Abbreviations
HCoVs, the human coronaviruses; M^{pro}, SARS-CoV-2 main protease; Neq1183, Nirmatrelvir; nsps, nonstructural proteins; OS, original strain; VOCs, variants of concern.

inhibitor Nirmatrelvir [12] and Ritonavir that inhibits cytochrome P4503A4 [13].

The SARS-CoV-2 virus has undergone various mutations since its first appearance, generating several variants of concern (VOCs): Alpha, Beta, Gamma, Delta, and Omicron [14]. The variants have generally shown a higher transmission efficiency and disease severity, which is related to mutations in the virus genome, more specifically in the spike protein [14]. The genomic sequences of the variants can be found in the Global Initiative on Sharing All Influenza website (https://gisaid.org). Although the majority of mutations are found in the spike protein, some mutations have also occurred in the M^{pro} sequence [15]. For this study, we specifically focused on two of the most widespread VOCs, Beta and Omicron. We sought to understand whether these mutations affect catalysis or specificity of M^{pro} using both synthetic peptide and protein-based substrates.

Results

SARS-CoV-2 M^{pro} construct

The M^{pro} mutations were performed by site-directed mutagenesis of the original strain (OS) M^{pro} construct (Fig. 1A). The beta mutations K90R and A193V are present at the domain I interface and, in a loop connecting domains II and III, respectively. The omicron mutation is present at domain II of the protein (Fig. 1B).

Kosmotropic salts lead to an increase in the original strain M^{pro} catalytic activity

As M^{pro} is an obligate dimer, we assumed that dimerization is concentration-dependent, obtaining satisfactory catalytic activity is necessary to increase the enzyme concentration. Kosmotropic salts have been employed routinely to investigate the dimeric status of enzymes *in vitro*, including other viral proteases and caspases [17,18]. To improve the enzyme's catalytic activity without having to work with high concentrations, the OS M^{pro} was tested against a series of kosmotropic salts, which are ions that have a stabilizing effect on proteins [19], and can lead to stabilization of dimeric conformations. The results showed that some kosmotropic salts, such as sodium citrate, were able to substantially enhance M^{pro} activity without the need for high concentrations of the enzyme in the assays.

The catalytic activity of M^{pro} is significantly increased in the presence of kosmotropes (Fig. 2). The most effective kosmotropic salt was sodium citrate, which is a known surrogate dimerization reagent [20,21]. The highest activity increase was observed when using 1.4 M of sodium citrate, which led to an increase in activity of 36.5-fold for the OS M^{pro} (Fig. 2B). Although, as the presence of sodium citrate can decrease the solubility of the inhibitors, a lower concentration of 0.7 M was chosen to use in the subsequent assays. Therefore, assays were performed in 20 mM PIPES pH 7.2, 100 mM NaCl and 1 mM EDTA buffer supplemented with 0.7 M citrate (assay buffer).

Mechanism of enhancement of activity by kosmotropes

To better understand the effects of sodium citrate on the catalytic activity of OS M^{pro}, the protease was assayed against the peptide substrate QS1 [22] using two concentrations of sodium citrate. The kinetic constants obtained for the OS M^{pro} using 1.0 and 0.7 M

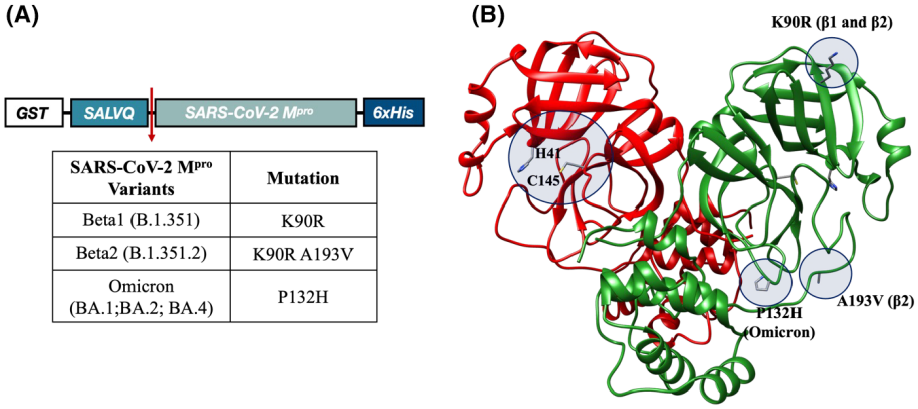

SARS-CoV-2 M^{pro} Variants	Mutation
Beta1 (B.1.351)	K90R
Beta2 (B.1.351.2)	K90R A193V
Omicron (BA.1;BA.2; BA.4)	P132H

Fig. 1. Graphical representation and structure of SARS-CoV-2 M^{pro}. (A) SARS-CoV-2 M^{pro} construct with the red arrow indicating the autocleavage during expression of the protein. The table displays the M^{pro} variants with the respective mutations on the protein sequence. (B) M^{pro} dimer structure, where the catalytic dyad C145 and H41 are displayed at protomer A (red), and the protein's mutations are highlighted in protomer B (green). The protein structure was generated using UCSF CHIMERA software [16]. PDB: 6WTM.

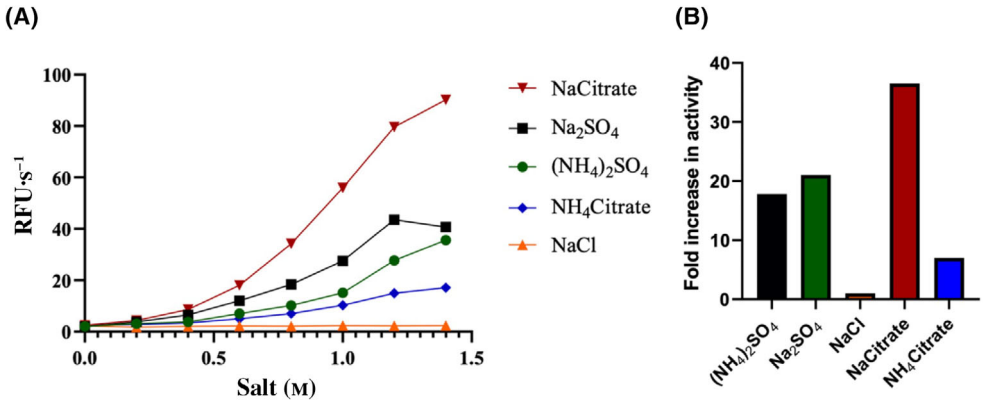

Fig. 2. Effect of kosmotropic salts on the activity of OS M^{pro}. (A) Rate of substrate QS1 cleavage over different concentrations of kosmotropes. (B) Fold increase in activity of OS M^{pro} at a salt concentration of 1.5 M. The fold increase was calculated by comparing the activity of the protease in a 20 mM PIPES pH 7.2 buffer with 100 mM of NaCl, 1 mM EDTA, and 4 mM DTT.

of sodium citrate revealed changes in both K_M and k_{cat}. The K_M values decreased by 3.6-fold as the concentration of sodium citrate increased, suggesting that the protein binds to the substrate with higher affinity. Similarly, the k_{cat} increases by 45-fold with the increase of sodium citrate. The data are consistent with the notion that sodium citrate enhances both the binding and catalysis, suggesting that the presence of sodium citrate leads to a better stabilization of the active conformation of the protein.

M^{pro} variants displayed similar catalytic efficiency on a peptide substrate

The M^{pro} variants were assayed against the peptide substrate QS1 to evaluate the effect of the mutations on the catalytic efficiency of the protease. The kinetic constants obtained for the variants showed that the mutations at the M^{pro} sequence led to a minimally improved catalytic efficiency for the QS1 substrate, with the Beta2 variant exhibiting at most a 1.5-fold increase in catalysis when compared to the OS M^{pro} (Fig. 3). We conclude that M^{pro} variants exhibit only minor differences in catalysis on the peptide substrate.

M^{pro} variants showed significantly increased catalytic efficiency on a protein substrate when compared to the original strain

To determine the influence of the M^{pro} mutations on a natural protein substrate, we constructed a protein that closely simulates the natural polyprotein environment, namely the catalytic mutant M^{pro}. This construct contains the catalytic C145 substituted by an alanine residue. The C145A M^{pro} has the same construct as the variants, with a sequence that mimics the natural substrate of M^{pro}. The assay is based on the fact that active M^{pro} will hydrolyze the catalytic

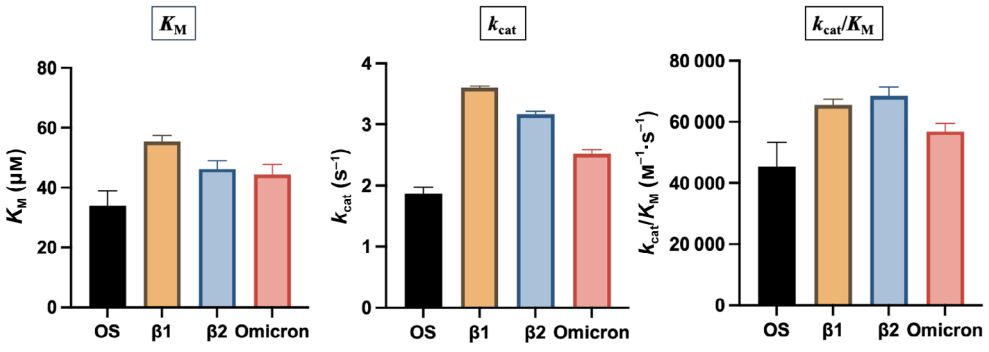

Fig. 3. Kinetic constant comparison of M^{pro} variants on a peptide substrate. Kinetic constants were obtained for the OS M^{pro} and variants in assay buffer against the substrate QS1 as described in Materials and methods. Values show the mean and standard deviation of three technical replicates.

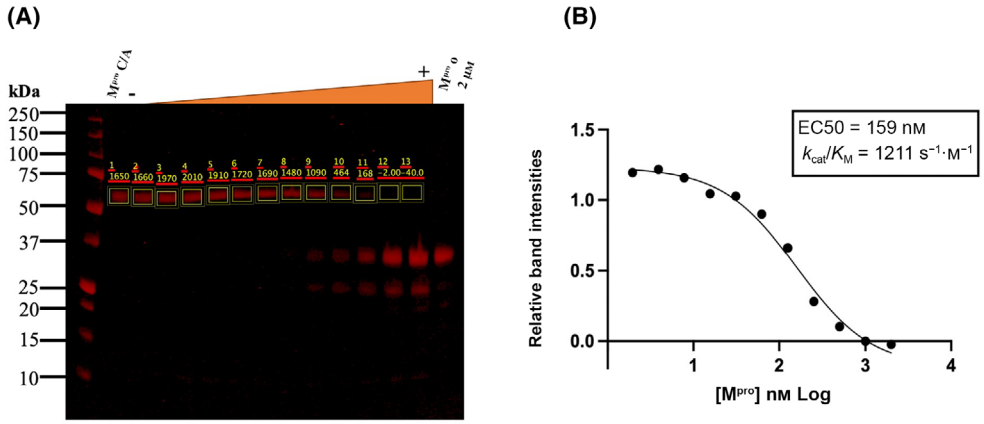

Fig. 4. Protein substrate cleavage by the omicron variant M^{pro}. (A) Densitometric analysis of the extent of cleavage of 2 μM protein substrate (catalytic mutant M^{pro}) by a twofold dilution series of the omicron variant in assay buffer for 1 h at 37 °C. This concentration was chosen for optimal visualization in the Coomassie-stained gel. (B) Relationship of relative band intensities against the omicron variant concentration reveals the EC50. Catalytic efficiency was calculated through Eqn (1) (see Materials and methods).

mutant M^{pro} at its recognition sequence SALVQ↓S, releasing the GST domain (Fig. 1A) which we visualized using SDS/PAGE (Fig. 4A). The SDS/PAGE gel was scanned, and through a densitometric analysis of the bands, the relative band intensities were plotted against the active protease concentration for the determination of the amount of enzyme required to cleave 50% of the substrate during the incubation period (EC50; Fig. 4B).

The results obtained for the protein-based substrate were considerably different than those for the peptide substrate (Fig. 5). The Beta2 variant had a higher catalytic efficiency than the Omicron variant with a substantial sevenfold increase in cleavage rate against the protein-based substrate when compared to the OS M^{pro}.

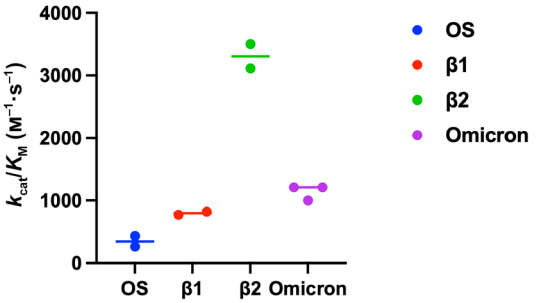

Fig. 5. Comparison of rate of cleavage of a protein-based substrate by M^{pro} variants. Two micromolar of the recombinant protein-based substrate was cleaved *in vitro* with a dilution series of the M^{pro} variants and analyzed by SDS/PAGE (as in Fig. 4). The k_{cat}/K_M values represent the mean and range of two to three independent measurements.

Inhibition of the M^{pro} variants is comparable with the original strain M^{pro}

We investigated the affinity of the M^{pro} variants with Nirmatrelvir (Neq1183) [12]. Binding was so tight that we were not able to observe equilibrium, and therefore, no K_i determination was possible. This is consistent with the covalent nature of the inhibitor [23]. Indeed, as the inhibitor had a similar behavior for all the M^{pro} variants and the enzyme concentrations were all equal to 25 nM, it was considered that the K_i for Neq1183 against the M^{pro} variants is below 25 nM, yielding a pK_i higher than 8.0, which is consistent with a previous publication [24]. All variants exhibited identical tight binding behavior with the inhibitor; therefore, we conclude that the inhibitor cannot distinguish between the variants.

Discussion

The objective of this study was to investigate the effects of different mutations in the SARS-CoV-2 sequence of the protease M^{pro} on the catalytic activity and specificity of this protease. Initial test with a fluorogenic peptide substrate (QS1) revealed that activity was substantially enhanced in the presence of kosmotropic salts. This is consistent with the need of M^{pro} to act as an obligate dimer [20,21]. In our study, the kosmotrope sodium citrate was able to improve the catalytic activity (k_{cat}/K_M) of the protease by 160-fold when compared to the M^{pro} activity in its conventional assay buffer (Table 1). This enhancement in activity resulted from an increase in both binding affinity (K_M) and turnover rate (k_{cat}).

Table 1. Effects of sodium citrate on kinetic constants. Kinetic constants were obtained for OS M^{pro} using PIPES pH 7.2 buffer with different concentrations of sodium citrate assayed with peptide substrate QS1. Different enzyme concentrations were used for differing sodium citrate concentrations as described in the table. The table shows the mean and standard deviation of three technical replicates.

[enzyme] (nM)	Sodium citrate (M)	K_M (μM)	k_{cat} (s^{-1})	k_{cat}/K_M (M^{-1} s^{-1})
200	0	182 ± 13	0.140 ± 0.003	778 ± 51
25	0.7	34 ± 4.9	1.87 ± 0.11	55 348 ± 4527
10	1.0	51 ± 2.3	6.30 ± 0.04	124 916 ± 5000

In optimal buffer, there were no substantial changes in the kinetic constants of the protease variants toward the peptide substrate QS1, suggesting that the mutations did not change the active site space enough to affect the enzymes' function [7]. In contrast, the protease variants were noticeably different when analyzed using a protein substrate. Thus, the mutations appear to have more impact on the overall structure of the protease, focusing on protein–protein interactions with its natural substrates, the nsps.

Since the activity of the variants on the peptide substrate was very similar, we hypothesized that peptide-based molecules would react similarly with all variants. This hypothesis was validated by testing with the inhibitor Neq1183. These results suggest that the mutations on the OS M^{pro} sequence, despite having a minor effect on a peptide substrate cleavage, did not change the catalytic site environment enough to build resistance to inhibition. Therefore, we propose that inhibitors initially designed for the M^{pro} of the original strain will be effective in all the variants. Hence, M^{pro} is likely to continue to be a target of therapeutic interest as mutations in its sequence are rare and, as we show here, have a minor effect on the protease's recognition of peptide-based molecules.

Materials and methods

Synthetic chemistry

Neq1183 was synthesized as per literature procedure [25] with minor modifications along route steps. The synthetic Scheme 1 and stepwise synthesis procedures are as follows.

To a solution of (1R,2S,5S)-methyl-6,6-dimethyl-3-azabicyclo[3.1.0]hexane-2-carboxylate HCl salt (1 equiv.) was added (S)-2-((tert-butoxycarbonyl)amino)-3,3-dimethylbutanoic acid (1.1 equiv.) in a mixture of DMF (2 mL) and acetonitrile (8 mL) at 0 °C was added HATU (1.1 equiv.) followed by dropwise addition of DIPEA (3 equiv.). The reaction mixture was allowed to warm to room temperature and stirred for 16 h. The reaction mixture was then concentrated, treated with water (20 mL), and extracted with ethyl acetate (3 × 25 mL). The combined organic phase was washed with HCl (1 M, 10 mL), brine, dried over Na_2SO_4, and evaporated under vacuum. The crude product was purified using flash silica gel chromatography (30–50% ethyl acetate in hexane) to afford the product as a colorless oil.

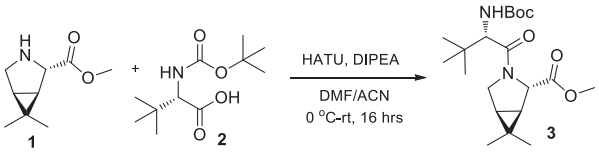

The methyl ester **3** (0.5 mmol) in 1 : 1 mixture of THF (3 mL) and aqueous 2 M LiOH (3 mL) was stirred at room temperature for 2 h. Then, the suspension was acidified with 2 M HCl to pH = 1 and extracted with ethyl acetate (3 × 25 mL). The combined organic phase was dried over sodium sulfate, filtered, and evaporated, and the crude product was used for the next step without purification.

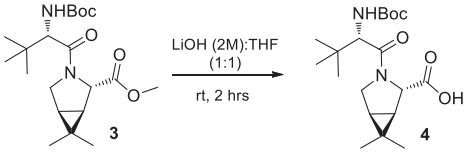

Triethylamine (3 equiv.) was added under argon to a solution of R-N-boc-3-methyl piperazine (1 equiv.) in dry dichloromethane, and the reaction mixture was cooled down to −78 °C. Trifluoroacetic anhydride (1 equiv.) was added dropwise, and the solution was stirred at −78 °C for 3 h. The reaction was quenched with a saturated aqueous solution of $NaHCO_3$ at −78 °C and was allowed to warm to room temperature. The aqueous phase was extracted with dichloromethane (3 × 25 mL), and the combined organic phase was washed with water (25 mL) dried over sodium sulfate, filtered, and concentrated under reduced pressure to obtain the product.

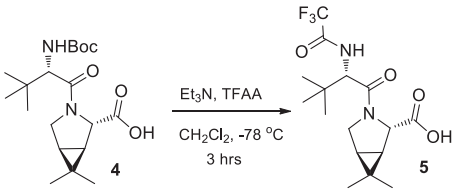

1-hydroxybenzotriazole hydrate (0.22 equiv.) was added to a solution of the acid **5** (1 equiv.) and the amine **6** (1.1 equiv.) in DMF. The mixture was cooled to 0 °C, and

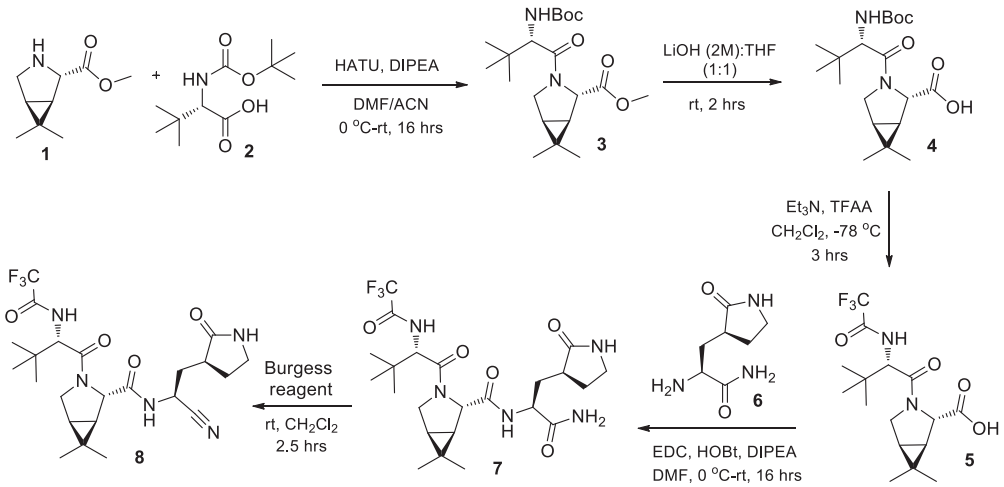

Scheme 1. Synthesis of Neq1183 starting with proline methyl ester analog.

DIPEA (3 equiv.) was added followed by EDC (1.2 equiv.). The resulting mixture was allowed to reach room temperature and was stirred at room temperature for 16 h. Then, this mixture was diluted with ethyl acetate (30 mL) and washed with water and brine. The organic phase was washed with 1 M HCl, brine, dried over sodium sulfate, filtered, and evaporated to afford the product.

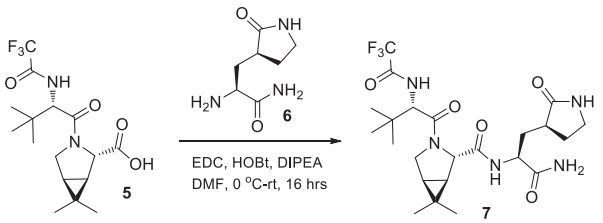

The amide 7 (1 equiv.) was dissolved in anhydrous dichloromethane and stirred at room temperature under argon. Burgess reagent (3.5 equiv.) was added in 50 mg portions over 2 h. The mixture was stirred for an additional 15 min, and the mixture was applied directly to silica gel for purification.

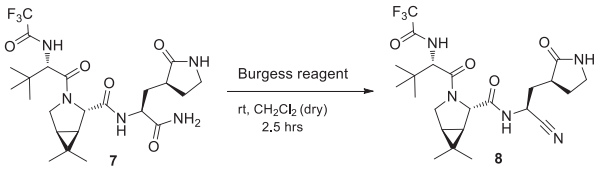

Neq1183 was obtained as a white solid. ^{1}H NMR (500 MHz, DMSO-*d6*) δ 9.39 (d, J = 8.3 Hz, 1H), 9.01 (d, J = 8.5 Hz, 1H), 7.65 (s, 1H), 4.96 (ddd, J = 10.9, 8.6, 5.2 Hz, 1H), 4.40 (d, J = 8.3 Hz, 1H), 4.14 (s, 1H), 3.90 (dd, J = 10.4, 5.5 Hz, 1H), 3.68 (d, J = 10.5 Hz, 1H), 3.35–3.45 (m, 2H), 3.13 (t, J = 9.1 Hz, 1H), 3.03 (dd, J = 16.5, 9.3 Hz, 1H), 2.39 (ddd, J = 19.1, 10.4, 4.4 Hz, 1H), 2.17–2.04 (m, 2H), 1.75–1.65 (m, 2H), 1.56 (dd, J = 7.5, 5.5 Hz, 1H), 1.14–1.09 (m, 1H), 0.97 (s, 9H), 0.87 (dd, J = 19.8, 12.2 Hz, 1H), 0.84 (s, 3H). HRMS (ESI+) [M + H] calculated for $C_{23}H_{33}F_3N_5O$ = 500.2485, found = 500.2507. The spectra and chromatograms are presented in the support information (Figs S1–S3).

Mutagenesis of SARS-CoV-2 M^{pro} variants

The SARS-CoV-2 M^{pro} plasmid was designed based on Zhang *et al.* [1] and inserted in a pGEX-6p-1 vector for expression in *Escherichia coli*. Mutations C145A, K90R (Beta1, Beta2), P132H (Omicron), and A193V (Beta2) were constructed by overlap PCR mutagenesis. The two internal, partially complementary, mutagenic primers were (forward, primer-1, 3, 5, and 7) and (reverse, primer-2, 4, 6, and 8; Table S1). The two flanking primers were (forward, primer-9) and (reverse, primer-10; Table S1). PCR was carried out on a GeneAmp PCR System 2400 (Perkin-Elmer, Waltham, MA, USA) with Phusion polymerase (Thermo Scientific, Waltham, MA, USA). The first round PCR generated two fragments using primer-9/primers-1,3,5,7 and primer-10/primers-2,4,6,8. The PCR products were purified by agarose gel, and the bands were excised and further purified using QIAquick PCR purification kit (Qiagen, Hilden, Germany). The purified products were combined and used as the template for the second round PCR with the two flanking primers. The PCR product was purified and restricted with *BamHI*/*XhoI*, purified again, and ligated to pGEX-6P-1 restricted with *BamHI*/*XhoI*. Competent cells of *E. coli* strain DH5α were transformed with the ligated vector. The full sequence of the insert was checked by DNA sequencing (Eton Biosciences, San Diego, CA, USA) to verify the success of the mutagenesis and the absence of

any other mutations. The expression plasmid was then subcloned into *E. coli* strain BL21(DE3) and expressed and purified as the original strain.

SARS-CoV-2 M^{pro} expression and purification

The construct has a GST tag at the N terminus that is connected to a linker with the recognition sequence that mimics the viral environment of the nonstructural proteins (nsps) for auto-cleavage during expression [8]. A C-terminal histidine tag was added to aid in purification.

The proteins were expressed using *E. coli* BL21 (DE3). Cultures were grown in 2× YT media containing 100 $\mu g \cdot mL^{-1}$ ampicillin (Sigma-Aldrich, Darmstadt, Germany). When cells reached an OD_{600} of 0.6, protein expression was induced with 0.5 mM of isopropyl-D-thiogalactoside (Sigma-Aldrich) at 37 °C, 100 ***g*** for 5 h. The cells were collected by centrifugation for 15 min at 9954 ***g*** and 4 °C. The obtained pellets were resuspended using lysis buffer A (20 mM Tris, 150 mM NaCl pH 7.8) in 5 $mL \cdot g^{-1}$ of pellet, and sonicated for 5 min. The lysate was centrifuged at 4 °C, 20 000 ***g*** for 1 h, and the obtained supernatant was added to a Ni^{2+}-chelating Sepharose resin (GE Healthcare Life Sciences, Chicago, IL, USA) on a chromatography column. Washed with 50 mL of buffer A and 10 mL of buffer B (20 mM Tris, 500 mM NaCl pH 7.8). The M^{pro}-His was obtained by imidazole elution using different percentages of buffer C (20 mM Tris pH 7.8, 150 mM NaCl, 500 mM Imidazole). The fractions were analyzed by SDS/PAGE. The protein samples were stored at −80 °C.

Enzyme kinetics

All assays were performed in a CLARIOstar microplate reader (BMG Labtech, Ortenberg, Germany) in a 96-well white plate (Corning New York, NY, USA), by following the release of 7-amino-4-carbamoylmethylcoumarin (ACC) fluorophore from the substrate Ac-Abu-Tle-Leu-Gln-ACC (QS1) [22] in an excitation and emission wavelength of 355 and 460 nm, respectively. The substrate hydrolysis rates ($RFU \cdot s^{-1}$) were determined and analyzed according to the methods below, which describe equilibrium and rate constants for the inhibition of M^{pro}.

Effect of kosmotropic salts on the M^{pro} activity

The OS M^{pro} activity was evaluated using different kosmotropic salts: sodium citrate (NaCitrate), ammonium citrate (NH_4Citrate), sodium sulfate ($NaSO_4$), ammonium sulfate ($(NH_4)_2SO_4$), and sodium chloride (NaCl). The assay was performed in buffer 20 mM PIPES, 100 mM NaCl, 1 mM EDTA, and 4 mM DTT pH 7.2. The enzyme (0.2 μM) samples were incubated into the buffer with different concentrations of kosmotropes in a range from 0 to 1.4 M. The substrate final concentration was 20 μM. The enzymatic assay was performed at 37 °C. The fluorescence emitted by the release of the ACC fluorophore was measured for approximately 15 min. Only the linear portion of each progress curve was used to determine the substrate hydrolysis rate in $RFU \cdot s^{-1}$.

Determination of the Michaelis–Menten constant (K_M) for OS SARS-CoV-2 M^{pro} and variants

The OS M^{pro} and variants were prepared in the assay buffer (20 mM PIPES pH 7.2, 100 mM NaCl, 1 mM EDTA, 0.7 M sodium citrate, 4 mM DTT). The final concentration of M^{pro} (25 nM) was titrated with serial dilutions of substrate. The rate of hydrolysis was monitored for approximately 15 min at 37 °C. Data were analyzed using (GRAPHPAD PRISM 8, San Diego, CA, USA).

Analysis of inhibition kinetics

The previously described M^{pro} inhibitor Neq1183 (Nirmatrelvir [12]) was titrated against the enzyme in assay buffer. The inhibitor was preincubated with M^{pro} (25 nM) for 30 min at 37 °C. The reaction was started with the addition of the QS1 substrate with a final concentration of 20 μM.

Cleavage of protein-based substrate

Cleavage of the protein substrate (catalytic mutant M^{pro}) was analyzed by observing the effect of a range of M^{pro} variant concentrations, by SDS/PAGE. The catalytic mutant M^{pro} was added to the protein solutions with a fixed concentration of 2.0 μM. The solutions were incubated for 1 h at 37 °C. After 1 h, the reaction was stopped by the addition of 30% TCA. Samples were boiled and added to an SDS/PAGE gel for the separation of the reaction products. The catalytic efficiency was obtained using Eqn (1) [21] by determining the M^{pro} concentration at which 50% of substrate cleavage was observed (EC50). The gels were scanned at 700 nm using a LI-COR Odyssey CLx.

Equation 1: k_{cat}/K_M determination for natural substrate cleavage. EC50 is the active M^{pro} concentration required to cleave half the substrate in the incubation period t.

$$k_{cat}/K_M = \frac{\ln 2}{(EC50)t} \quad (1)$$

Acknowledgements

We thank the Fulbright Commission Brazil for the funding. We thank the Fundação de Amparo a Pesquisa do Estado de São Paulo—FAPESP (grant #2022/01393-5) and Coordenação de Aperfeiçoamento

de Pessoal de Nível Superior (CAPES) for the financial support. The Drag laboratory is supported by the '-TEAM/2017-4/32' project, which is conducted within the TEAM program of the Foundation for Polish Science co-financed by the European Union under the European Regional Development Fund.

Conflict of interest

The authors declare no conflict of interest.

Author contributions

FRR, SJS, and GSS conceived the study. FRR wrote the manuscript and performed the protein expression and all the kinetic experiments. SJS performed the mutagenesis. AS performed the inhibitor synthesis. WR designed and synthesized the fluorogenic substrate. CAM and MD contributed to data analysis and suggestions.

Peer review

The peer review history for this article is available at https://www.webofscience.com/api/gateway/wos/peer-review/10.1111/febs.16970.

Data availability statement

All data needed to evaluate the conclusion of the paper are present in the paper and can be found in the Supporting Information. Source data of this study are available from the corresponding author upon request.

References

1 Zhang L, Lin D, Sun X, Curth U, Drosten C, Sauerhering L, Becker S, Rox K & Hilgenfeld R (2020) Crystal structure of SARS-CoV-2 main protease provides a basis for design of improved α-ketoamide inhibitors. *Science* **368**, 409–412.
2 Jin Z, Du X, Xu Y, Deng Y, Liu M, Zhao Y, Zhang B, Li X, Zhang L, Peng C *et al.* (2020) Structure of Mpro from SARS-CoV-2 and discovery of its inhibitors. *Nature* **582**, 289–293.
3 Hilgenfeld R (2014) From SARS to MERS: crystallographic studies on coronaviral proteases enable antiviral drug design. *FEBS J* **281**, 4085–4096.
4 Thiel V, Herold J, Schelle B & Siddell SG (2001) Viral replicase gene products suffice for coronavirus discontinuous transcription. *J Virol* **75**, 6676–6681.
5 Dai W, Zhang B, Su H, Li J, Zhao Y, Xie X, Jin Z, Liu F, Li C, Li Y *et al.* (2020) Structure-based design of antiviral drug candidates targeting the SARS-CoV-2 main protease. *Science* **368**, 1331–1335.
6 Minkoff JM & tenOever B (2023) Innate immune evasion strategies of SARS-CoV-2. *Nat Rev Microbiol* **21**, 178–194.
7 Chen SA, Arutyunova E, Lu J, Khan MB, Rut W, Zmudzinski M, Shahbaz S, Iyyathurai J, Moussa EW, Turner Z *et al.* (2023) SARS-CoV-2 M^{pro} protease variants of concern display altered viral substrate and cell host target Galectin-8 processing but retain sensitivity toward antivirals. *ACS Cent Sci* **9**, 696–708.
8 Miltner N, Kalló G, Csősz É, Miczi M, Nagy T, Mahdi M, Mótyán JA & Tőzsér J (2023) Identification of SARS-CoV-2 Main protease (M^{pro}) cleavage sites using two-dimensional electrophoresis and in silico cleavage site prediction. *Int J Mol Sci* **24**, 3236.
9 Brewitz L, Dumjahn L, Zhao Y, Owen CD, Laidlaw SM, Malla TR, Nguyen D, Lukacik P, Salah E, Crawshaw AD *et al.* (2023) Alkyne derivatives of SARS-CoV-2 Main protease inhibitors including Nirmatrelvir inhibit by reacting covalently with the nucleophilic cysteine. *J Med Chem* **66**, 2663–2680.
10 Previti S, Ettari R, Calcaterra E, Di Maro S, Hammerschmidt SJ, Müller C, Ziebuhr J, Schirmeister T, Cosconati S & Zappalà M (2023) Structure-based lead optimization of peptide-based vinyl methyl ketones as SARS-CoV-2 main protease inhibitors. *Eur J Med Chem* **247**, 115021.
11 Lamb YN (2022) Nirmatrelvir plus ritonavir: first approval. *Drugs* **82**, 585–591.
12 Owen DR, Allerton CMN, Anderson AS, Aschenbrenner L, Avery M, Berritt S, Boras B, Cardin RD, Carlo A, Coffman KJ *et al.* (2021) An oral SARS-CoV-2 M^{pro} inhibitor clinical candidate for the treatment of COVID-19. *Science* **374**, 1586–1593.
13 Sevrioukova IF & Poulos TL (2010) Structure and mechanism of the complex between cytochrome P4503A4 and ritonavir. *Proc Natl Acad Sci USA* **107**, 18422–18427.
14 Jacobs JL, Haidar G & Mellors JW (2023) COVID-19: challenges of viral variants. *Annu Rev Med* **74**, 31–53.
15 Hu Y, Lewandowski EM, Tan H, Zhang X, Morgan RT, Zhang X, Jacobs LMC, Butler SG, Gongora MV, Choy J *et al.* (2022) Naturally occurring mutations of SARS-CoV-2 main protease confer drug resistance to nirmatrelvir. *ACS Cent Sci* **9**, 1658–1669.
16 Pettersen EF, Goddard TD, Huang CC, Couch GS, Greenblatt DM, Meng EC & Ferrin TE (2004) UCSF Chimera—a visualization system for exploratory research and analysis. *J Comput Chem* **25**, 1605–1612.
17 Boatright KM, Renatus M, Scott FL, Sperandio S, Shin H, Pedersen IM, Ricci J-E, Edris WA, Sutherlin DP, Green DR *et al.* (2003) A unified model for apical caspase activation. *Mol Cell* **11**, 529–541.

18 Schmidt U & Darke PL (1997) Dimerization and activation of the herpes simplex virus type 1 protease. *J Biol Chem* **272**, 7732–7735.
19 Okur HI, Hladílková J, Rembert KB, Cho Y, Heyda J, Dzubiella J, Cremer PS & Jungwirth P (2017) Beyond the Hofmeister series: ion-specific effects on proteins and their biological functions. *J Phys Chem B* **121**, 1997–2014.
20 Okamoto DN, Oliveira LCG, Kondo MY, Cezari MHS, Szeltner Z, Juhász T, Juliano MA, Polgár L, Juliano L & Gouvea IE (2010) Increase of SARS-CoV 3CL peptidase activity due to macromolecular crowding effects in the milieu composition. *Biol Chem* **391**, 1461–1468.
21 Pop C, Fitzgerald P, Green DR & Salvesen GS (2007) Role of proteolysis in Caspase-8 activation and stabilization. *Biochemistry* **46**, 4398–4407.
22 Rut W, Groborz K, Zhang L, Sun X, Zmudzinski M, Pawlik B, Wang X, Jochmans D, Neyts J, Møynarski W *et al.* (2021) SARS-CoV-2 Mpro inhibitors and activity-based probes for patient-sample imaging. *Nat Chem Biol* **17**, 222–228.
23 Bonatto V, Lameiro RF, Rocho FR, Lameira J, Leitão A & Montanari CA (2023) Nitriles: an attractive approach to the development of covalent inhibitors. *RSC Med Chem* **14**, 201–217.
24 Greasley SE, Noell S, Plotnikova O, Ferre R, Liu W, Bolanos B, Fennell K, Nicki J, Craig T, Zhu Y *et al.* (2022) Structural basis for the in vitro efficacy of nirmatrelvir against SARS-CoV-2 variants. *J Biol Chem* **298**, 101972.
25 Owen DR, Petersson MY, Reese MR, Sammons MF, Tuttle JB, Verhoest PR, Wei L, Yang Q & Yang X (2021) Nitrile-containing antiviral compounds. WO Patent, WO2021/250648 A1, December 2021.

Supporting information

Additional supporting information may be found online in the Supporting Information section at the end of the article.

Fig. S1. HPLC chromatogram Neq1183 (CHIRALPAK IB 4.6 × 250 mm, 5 mic, gradient 5–100% of B in 30 min.

Fig. S2. ^{1}HNMR spectrum of Neq1183 (500 MHz, DMSO-d6).

Fig. S3. High-resolution mass spectrogram of Neq1183.

Table S1. Primers for SARS-CoV-2 M^{pro} PCR mutagenesis.